Resonance Raman Spectra of Manganese Myoglobin and Its Azide Complex. Assignment of a New Charge-Transfer Band to Azide (π) → Porphyrin (π^*) Transition†

Nai-Teng Yu* and Motonari Tsubaki

ABSTRACT: The enhancement of bound azide vibrations at 650 [depolarized (dp), bending] and 2039 cm^{-1} (dp, antisymmetric stretch) upon excitation at ~400–460 nm indicates the existence of a new charge-transfer transition in manganese(III) myoglobin–azide complex. The assignments of these two vibrational modes are based on the agreement of their $^{15}N_3$ isotope shifts (22 and 70 cm^{-1}) with the calculated values (22 and 69 cm^{-1}), the depolarized nature, and their close proximity to the corresponding vibrations in ionized azide. The Mn(III)–N_3 stretch has not been observed in the present study although the Fe(III)–N_3 stretch at 413 cm^{-1} (polarized) was reported [Asher, S. A., Vickery, L. E., Schuster, T. M., & Sauer, K. (1977) *Biochemistry 16*, 5849]. The RR spectra of Mn^{III}Mb–azide between 150 and 300 cm^{-1} differ dramatically from those of Fe^{III}Mb–azide excited in the 640-nm charge-transfer band or near the Soret band. There are lines at 170 and 282 cm^{-1} (both polarized) in the Mn^{III}Mb–azide spectra which exhibit extremely large resonance enhancements and are unshifted by $^{15}N_3$ isotope substitution. These two lines, having no analogue in other heme protein spectra, may be tentatively assigned to the out-of-plane porphyrin ring vibrations, with the latter involving significant Mn(III)–N(pyrrole) stretch. The enhancement of non totally symmetric azide modes suggests that the charge-transfer state may be mixed with other excited electronic states (possibly band Va or band VI) via Herzberg–Teller vibronic couplings. The lack of enhancement of the Mn(III)–N_3 stretch leads to our present assignment of azide (π) → porphyrin (π^*) charge-transfer transition rather than azide (π) → metal (d_{z^2}) or azide (n) → metal (d_{z^2}).

It is generally recognized that resonance Raman spectra of the prosthetic group of heme proteins, excited in the Q (visible) and B (Soret) regions, permit one to obtain structural information concerning core expansion/metal displacement, doming, spin-state equilibrium, and iron oxidation state (Spaulding et al., 1975; Yu, 1977; Spiro & Strekas, 1974; Spiro et al., 1979; Asher & Schuster, 1979). However, Raman lines so enhanced are confined to the porphyrin ring vibrations, and information pertaining to axial ligands cannot be obtained. Recently, attention has begun to focus on possible resonance with states other than the dominant Q and B states. Asher et al. (1977, 1979) in their studies of metmyoglobin and methemoglobin derivatives have shown that iron–axial ligand stretching modes may be selectively enhanced by weak absorption bands near 600–640 nm which may be due to ligand → Fe(III) charge-transfer transitions. Desbois et al. (1979) were able to bring out several iron–axial ligand stretches in myoglobin derivatives, possibly in resonance with the underlying charge-transfer transitions near the Soret band. On the other hand, Wright et al. (1979) employed resonance Raman excitation profiles to locate a new charge-transfer band at 490 nm in bis(pyridine)iron(II) mesoporphyrin IX dimethyl ester, which was assigned to the Fe (d_π) → pyridine (π^*) transition. In resonance with this charge-transfer state, totally symmetric (but not non totally symmetric) internal pyridine vibrational modes as well as the Fe–py stretch are greatly enhanced, consistent with the one-state Franck–Condon scattering mechanism.

Thus, resonance Raman scattering appears to be a powerful tool for the study of charge-transfer transitions in metalloporphyrins and heme proteins. Unlike infrared spectroscopy, RR scattering is not restricted to a spectral "window" for the observation of bound ligand vibrations (McCoy & Caughey, 1970). It provides not only the ground-state vibrational frequencies but also important information related to the nature of charge-transfer transitions so that interactions between heme and ligands may be better understood.

Manganese-substituted hemes are of particular interest for resonance Raman studies because their absorption spectra are so drastically different from those of iron hemes. Instead of an intense B (Soret) band at ~410 nm, the Mn(III) hemes exhibit "split Soret" absorptions at ~460 (band V) and ~370 nm (band VI). The origin of the extra band (band V) has been ascribed to a porphyrin ring to Mn(III) charge-transfer transition (Boucher, 1972). Gaughan et al. (1975) studied the resonance Raman spectra of the manganese(III) tetraphenylporphyrin–halide complex by excitation within band V and were in favor of a charge-transfer assignment to band V. Further investigation on the halide complex of manganese(III) etioporphyrin I was performed by Asher & Sauer (1976), who claimed the observation of Mn(III)–X stretches (where X = F^-, Cl^-, Br^-, and I^-) upon excitation in the band V region, which was taken as evidence for charge-transfer character in band V. However, Shelnutt et al. (1976) interpreted the excitation profile of the manganese(III) etioporphyrin–halide complex as indicating $\pi \rightarrow \pi^*$ character in band V.

In this paper, we report the resonance Raman studies of the Mn(III) form of the manganese-substituted myoglobin (Mn^{III}Mb) and its azide complex ($Mn^{III}Mb{\cdot}N_3^-$) upon excitation around band V. Excitation profiles of bound azide modes indicate a new charge-transfer transition located between bands V and VI, which is assigned as the azide (π) → porphyrin (π^*) type. Non totally symmetric internal azide vibrations at 650 (bending) and 2039 cm^{-1} (antisymmetric stretch) are enhanced by vibronic couplings between this charge-transfer state and nearby excited electronic states. This may be the first observation of resonance-enhanced non totally

† From the School of Chemistry, Georgia Institute of Technology, Atlanta, Georgia 30332. *Received April 1, 1980.* This work was supported in part by grants (GM 18894 and EY 01746) from the National Institutes of Health.

* Correspondence should be addressed to this author. Recipient of National Institutes of Health Research Career Development Award EY 00073.

0006-2960/80/0419-4647$01.00/0

symmetric bound ligand modes in hemoproteins. Low-frequency RR spectra of $Mn^{III}Mb{\cdot}H_2O$ excited in band V are very similar to $Fe^{III}Mb{\cdot}H_2O$ excited in the Soret band, indicating that band V in Mn^{3+} protein is mainly a Soret-like ($\pi \rightarrow \pi^*$) transition.

Materials and Methods

Manganese protoporphyrin IX was prepared according to Yonetani & Asakura (1969) and was purified on a column of silica gel (Fisher, 100–200 mesh, grade 923) developed with the lower layer of a mixture of pyridine–chloroform–water–isooctane (50:25:25:2.5 v/v).

Sperm whale myoglobin was purchased from Sigma Chemical Co. The lyophilized powder was dissolved in 0.01 M sodium phosphate buffer, pH 6.9 ($NaH_2PO_4{\cdot}2H_2O$, 2.26 g; Na_2HPO_4, 2.52 g/5 L), and gel-filtered against the same buffer. The myoglobin solution was then applied to a column of CM-52 cellulose (Whatman) equilibrated with the same buffer. After washing, the adsorbed myoglobin main component was slowly eluted by 0.025 M sodium phosphate buffer, pH 7.2 ($NaH_2PO_4{\cdot}H_2O$, 1.000 g; Na_2HPO_4, 1.325 g/L).

The heme group was removed from metmyoglobin by the procedure of Teale (1959) by using 2-butanone. The incorporation of manganese protoporphyrin IX into apoMb was carried out by the method of Sono & Asakura (1975). The reconstituted Mb was further purified in the oxidized form by the same procedure used for native myoglobin.

The MnMb concentration was determined spectrophotometrically by using the extinction coefficient of 70 mM^{-1} cm^{-1} at 468 nm as reported by Hoffman & Gibson (1976).

Before Raman experiments, 0.40 mL of $Mn^{III}Mb$ solution (0.14 mM; 0.05 M sodium phosphate buffer, pH 7.2) was passed through a Millipore filter (pore size 0.45 μm). The azide complex was prepared by adding solid sodium azide (Fisher) directly into the solution of $Mn^{III}Mb$, and the pH value was then measured and adjusted. Triply labeled $Na^{15}N_3$ (99 atom %) and terminally labeled $K^{14}N^{14}N^{15}N$ (99.4 atom %) were purchased from Stohler Isotope Chemicals and Prochem, respectively. Reduced MnMb was prepared from the oxidized form in the rubber-sealed Raman cell by repeated evacuation, flushing with N_2 gas, and finally adding concentrated sodium dithionite solution anaerobically.

Raman spectra were obtained by using a cooled SIT-detected multichannel Raman system (Yu & Srivastava, 1980). This spectrometer allows one to acquire a large segment (~400–700 cm^{-1}) of the Raman spectrum without mechanical scanning of the gratings. The SIT is controlled by a microprocessor-based OMA 2 (optical multichannel analyzer from Princeton Applied Research) which permits data storage and analysis. To optimize the resolution and spectral bandpass, we have employed a 0.85-m Czerny-Turner double monochromator in additive dispersion (two 600 groves/mm gratings). This system was shown to be ghost-free.

The Raman cell was kept in a rotating cell holder for laser irradiation, and a 90° scattering geometry was used. Exciting wavelengths at 528.7, 514.5, 501.7, 496.5, 488.0, 476.5, 472.7, 465.8, and 457.9 nm were provided by an argon ion laser (CR-8) and those at 568.2, 530.9, 520.8, 413.1, and 406.7 nm by a krypton ion laser (Spectra Physics Model 171/01 or CR-500K).

The spectra obtained at each "window" were calibrated by using fenchone, indene, CN^-, and 1,2-butadiene as standard compounds by a special cubic fitting function in the OMA 2 console. A conventional Raman system (Spex 1401 double monochromator and photon-counting electronics) was used for excitation profile measurements. This system allows one to obtain continuous Raman spectra of $Mn^{III}Mb{\cdot}N_3^-$ in the 100–1700-cm^{-1} region. Excitation profiles were constructed by using sulfate ion line at 983 cm^{-1} (0.30 M ammonium sulfate) as an internal standard. No correction for self-absorption was made because we place the laser beam very close to the glass–solution interface (within 0.10 mm from the glass surface). The decrease of the scattered light intensity due to self-absorption is less than 10% at the absorption maximum (470 nm). All the wavenumbers reported here are accurate within ±2 cm^{-1}.

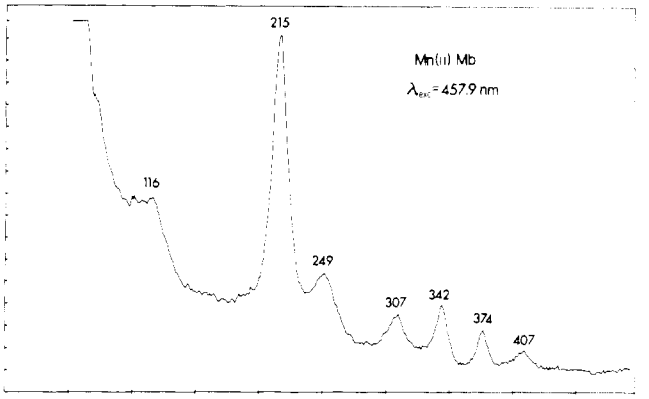

FIGURE 1: Lower frequency region RR spectrum of $Mn^{II}Mb$. Excitation wavelength (λ), 457.9 nm; laser power (p), 15 mW; slit width (σ), 200 μm; data integration time (τ), 303 s (10000 delay cycles, 100 readout scans); heme concentration (c), 0.14 mM in 0.025 M sodium phosphate buffer.

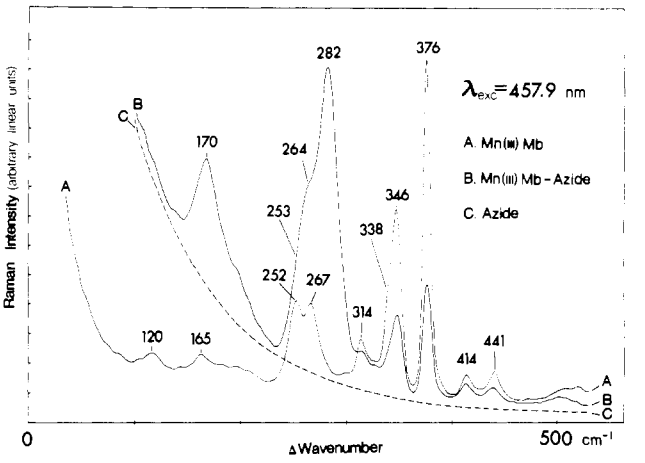

FIGURE 2: Lower frequency region RR spectra of $Mn^{III}Mb{\cdot}H_2O$ (curve A) and $Mn^{III}Mb{\cdot}N_3^-$ (curve B). Conditions: λ, 457.9 nm; p, 8 mW; σ, 100 μm; 0.20 M $Na^{14}N_3$; τ, 303 s.

Results

In the reduced state of manganese myoglobin, the electronic absorption spectrum loses its anomaly and displays an intense single Soret band at ~440 nm. As shown in Figure 1, the RR spectrum of $Mn^{II}Mb$ is essentially similar to that of deoxy-$Fe^{II}Mb$, reported by Desbois et al. (1979), Kincaid et al. (1979a,b), Kitagawa et al. (1979), and Tsubaki et al. (1980). These authors observed lines at 220, 240 (shoulder), 304, 344, 372, and 406 cm^{-1} (within the accuracy of ±2 cm^{-1}), which correspond to 215, 249, 307, 342, 374, and 407 cm^{-1} in Figure 1. There is a line at 438 cm^{-1} in the spectrum of $Fe^{II}Mb$ which is extremely weak in $Mn^{II}Mb$. In addition, a new low-frequency mode appears at 116 cm^{-1} in Figure 1.

Figure 2 shows typical RR spectra of $Mn^{III}Mb{\cdot}H_2O$ and $Mn^{III}Mb{\cdot}N_3^-$ (200 mM azide ion concentration). These spectra were obtained with excitation at 457.9 nm which is on the high-energy side of band V (Figure 3). The

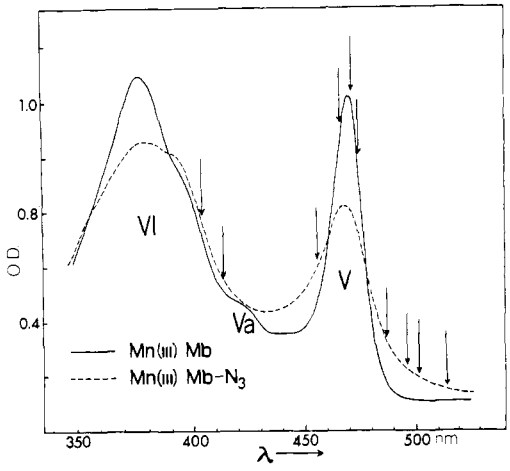

FIGURE 3: Absorption spectra of $Mn^{III}Mb$ (—) and $Mn^{III}Mb$–azide complex (- - -). Concentrations: 0.014 mM $Mn^{III}Mb$; 0.5 M azide ion. The arrow indicates the locations of various laser wavelengths used in this work.

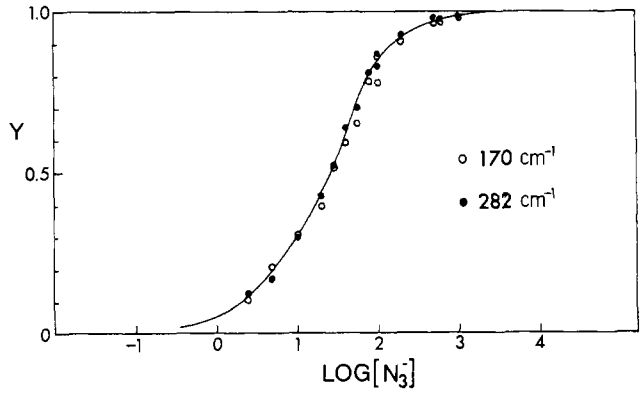

FIGURE 4: Azide binding curve at $Mn^{III}Mb$ concentrations of 0.14 mM in 0.025 M sodium phosphate buffer, pH 7.2, at room temperature (25 °C). Data were obtained from the 170-cm^{-1} mode (○) and 282-cm^{-1} mode (●).

$Mn^{III}Mb{\cdot}H_2O$ spectrum presented here is well resolved and appears to be qualitatively similar to that of $Fe^{III}Mb{\cdot}H_2O$ reported by Desbois et al. (1979) using near-Soret excitation. They observed lines at 249, 272, 308, 346, 378, 411, and 442 cm^{-1}, corresponding to our present lines of $Mn^{III}Mb{\cdot}H_2O$ at 252, 267, 314, 346, 376, 414, and 441 cm^{-1}, respectively.

The near-Soret-excited RR spectrum of $Fe^{III}Mb{\cdot}N_3^-$ is essentially similar to that of $Fe^{III}Mb{\cdot}H_2O$ except for the 570 cm^{-1} line which was assigned to the Fe–N_3 stretching vibration by Desbois et al. (1979). However, the spectrum of $Mn^{III}Mb{\cdot}N_3^-$ shows different features, two strong polarized lines at 170 and 282 cm^{-1}, but no line near 570 cm^{-1}. Free azide ion does not give rise to Raman lines in this region (50–600 cm^{-1}), but contributes to the sloping background as indicated by the dashed line in Figure 2.

A plot of fractional saturation (Y) vs. azide ion concentration (mM) is shown in Figure 4. This apparent azide binding curve was obtained indirectly from relative intensity ratios (K) between 170- (or 282-) and 376-cm^{-1} modes as a function of azide concentration (with excitation at 457.9 nm). The intensity ratio (K) is related to the fractional saturation (Y) by

$$K = \frac{I(1 - Y) + I'Y}{I_{376}(1 - Y) + I'_{376}Y}$$

where I and I' are intrinsic Raman scattering coefficients at 170 or 282 cm^{-1} for $Mn^{III}Mb{\cdot}H_2O$ and $Mn^{III}Mb{\cdot}N_3^-$, respectively; I_{376} and I'_{376} are the corresponding coefficients as measured at 376 cm^{-1}. The value of Y for each measurement of K was calculated from the ratios I/I_{376}, I'/I'_{376}, and I_{376}/I'_{376}. The first and second ratios were determined under 0% and 100% saturation (extrapolated), while the third ratio required the use of a cacodylic line (at 608 cm^{-1}) as an internal intensity standard. The necessity of such an indirect method was caused by the lack of a suitable standard line in the 100–550-cm^{-1} "window" region where the 170- and 282-cm^{-1} lines appeared. The concentration for half-saturation in Figure 3 is ca. 20 mM, which is consistent with the value reported by Hoffman & Gibson (1976) for room temperature.

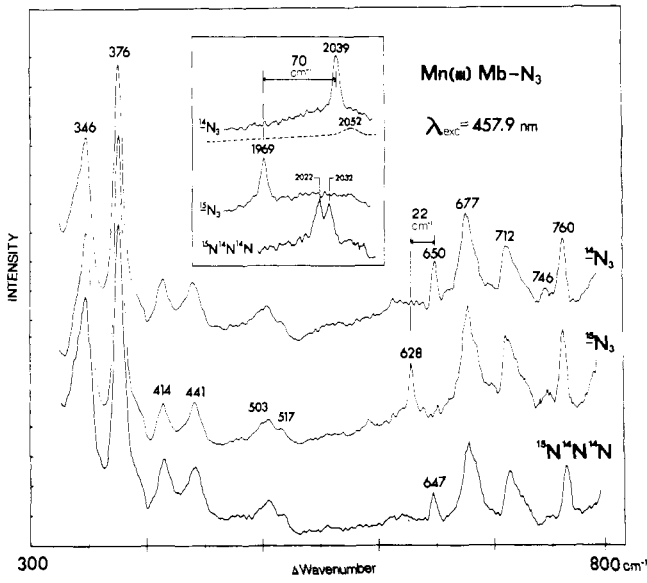

FIGURE 5: RR spectra of $^{14}N_3$, $^{15}N_3$, and $^{15}N^{14}N^{14}N$ derivatives of $Mn^{III}Mb$ in the 300–800-cm^{-1} and 1900–2100-cm^{-1} regions (inset). Conditions: λ, 457.9 nm; p, 30 mW; σ, 50 μm for 300–800-cm^{-1} and 100 μm for 1900–2100-cm^{-1} regions; 0.25 M $Na^{14}N_3$, $Na^{15}N_3$, and $K^{15}N^{14}N^{14}N$; τ, 303 s.

With excitation at 476.5 nm near the band V maximum, the intensities of the lines at 170 and 282 cm^{-1} were greatly reduced so that the 252- and 267-cm^{-1} lines were clearly observed even at 1.0 M azide ion concentration. In other words, these two lines along with those at 314, 338, 346, 376, 414, and 441 cm^{-1} do not disappear upon azide binding. The strong lines at 170 and 282 cm^{-1} in the spectrum of $Mn^{III}Mb{\cdot}N_3^-$ cannot be identified as Mn(III)–N_3 stretch or any modes associated with azide motion, because they are unshifted (within ±2 cm^{-1}) by $^{15}N_3$ isotope substitution.

Two isotope sensitive lines were found at 650 and 2039 cm^{-1} (Figure 5). The 650-cm^{-1} line shifted 22 cm^{-1} to lower energy when $^{14}N_3$ was substituted by $^{15}N_3$. A 3-cm^{-1} shift was observed upon substitution by terminally labeled $^{15}N^{14}N^{14}N$. The bending vibration of azide ion in metal azide has been reported to occur around 650 cm^{-1} from infrared spectroscopy (LiN_3, 635 cm^{-1}; NaN_3, 639 cm^{-1}; KN_3, 645 cm^{-1}; RbN_3, 642 cm^{-1}; CsN_3, 635 cm^{-1}; see Jones, 1973), although we could not observed any Raman signal from free azide ion in this region (non resonance Raman inactive). The infrared spectrum of the iron(III) octaethylporphyrin–azide complex showed the azide bending vibration at 629 cm^{-1} (Ogoshi et al., 1973), very close in energy to 650 cm^{-1}. These data do suggest the possible assignment of this 650-cm^{-1} line to the resonance-enhanced internal azide bending mode. When a linear triatomic harmonic oscillator model is used, the predicted frequency shifts are 22 cm^{-1} upon substitution by triply labeled azide and 4 cm^{-1} by terminally labeled azide. These values are in good agreement with the observed ones. Furthermore, our polar-

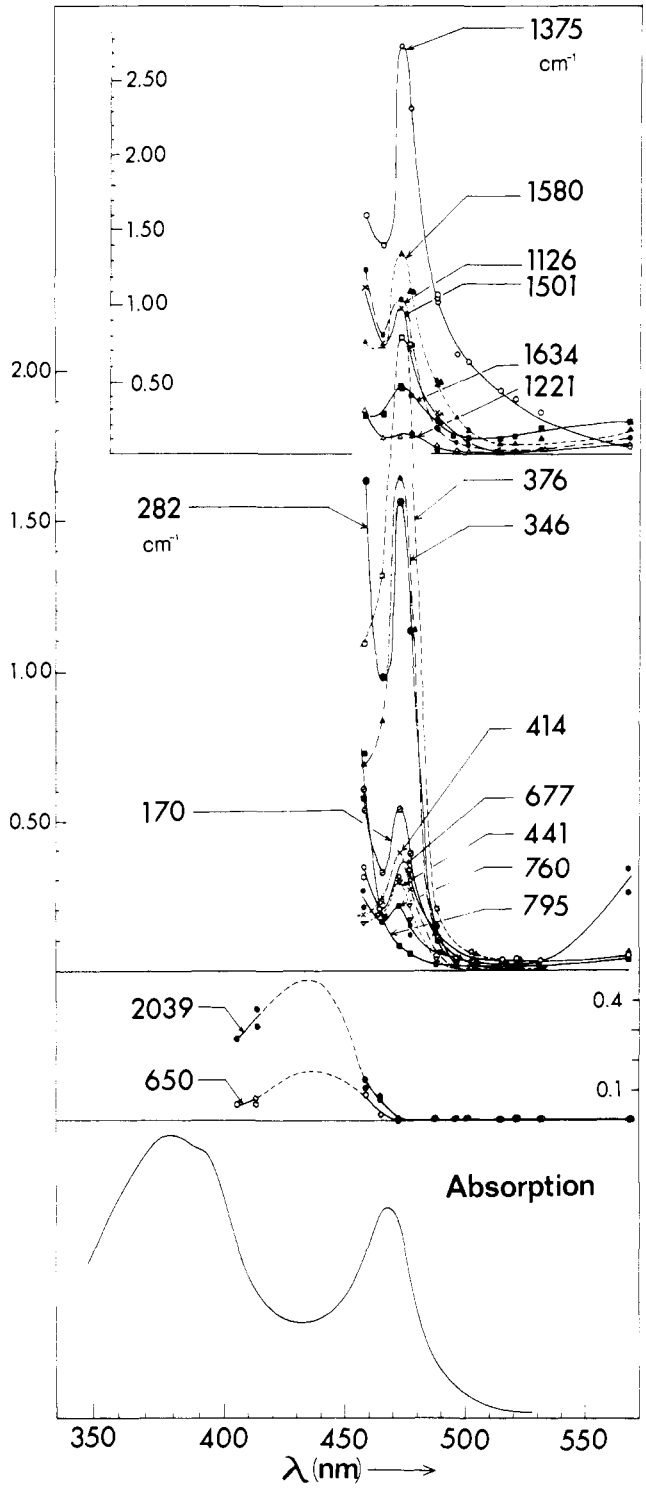

FIGURE 6: Excitation profiles of major Raman lines of $MN^{III}Mb{\cdot}N_3^-$ near band V and band VI absorption maxima. Conditions: σ, 400 μm; scan speed, 0.5 cm^{-1}/s; ligand concentration 0.25 M $Na^{14}N_3$; other sample conditions are the same as in Figure 1. The data points for 650- and 2039-cm^{-1} lines upon excitation at 413.1 and 406.7 nm were obtained within ~5 min of irradiation before significant accumulation of new complexes (photoinduced).

ization measurements indicated that the 650-cm^{-1} line is depolarized, as is expected for an internal azide bending mode. On the other hand, the 2039-cm^{-1} line exhibited a shift of 70 cm^{-1} to lower frequency upon $^{15}N_3$ substitution, in good agreement with the calculated shift of 69 cm^{-1}. It is clearly assignable to the internal azide antisymmetric stretching mode. If we assume no interaction between the azide antisymmetric

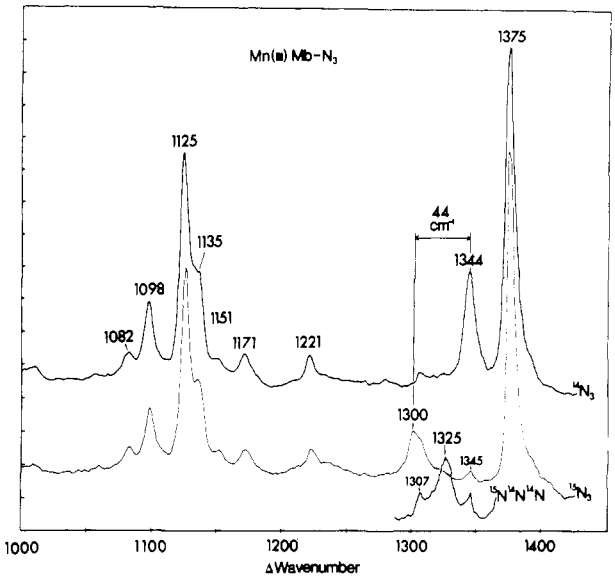

FIGURE 7: RR spectra of $^{14}N_3$, $^{15}N_3$, and $^{15}N^{14}N^{14}N$ derivatives of $Mn^{III}Mb$ in the 1000–1400-cm^{-1} region. Conditions: λ, 457.9 nm; p, 7 mW; σ, 200 μm; ligand concentration, 0.5 M $Na^{14}N_3$, $Na^{15}N_3$, and $K^{15}N^{14}N^{14}N$; other conditions same as in Figure 1.

stretch and other coordinates, the 2039-cm^{-1} line should show an 11-cm^{-1} shift to 2028 cm^{-1} upon $^{15}N^{14}N^{14}N$ substitution. Instead, we observed a doublet (at 2022 and 2032 cm^{-1}) of equal intensity which may be ascribed to the inequivalency of the two terminal nitrogens as a result of interaction between azide and manganese(III) porphyrin. X-ray crystallographic studies on $Fe^{III}Mb{\cdot}N_3^-$ and $Fe^{III}Hb{\cdot}N_3^-$ indicated that triatomic azide ion binds iron with a bend coordination (the Fe–N–N angles being 111 and 125°, respectively) (Stryer et al., 1964; Perutz & Mathews, 1966; Deatherage et al., 1979). X-ray data on manganese(III) tetraphenylporphyrin–azide complexes also showed azide binding in a bent configuration (Day et al., 1974, 1975). It is quite possible that such a configuration is preserved in the azide binding to $Mn^{III}Mb$. An internal azide antisymmetric stretch of $Fe^{III}Mb{\cdot}N_3^-$ for both low- and high-spin states was observed at 2023 and 2046 cm^{-1}, respectively, by infrared spectroscopy (McCoy & Caughey, 1970; Alben and Fager, 1972). It is noteworthy that the 2039-cm^{-1} line of $Mn^{III}Mb{\cdot}N_3^-$ is located between these two frequencies, although manganese(III) porphyrin complexes are known to be high spin ($S = 2$), independent of ligand form.

In Figure 6 we compare the excitation profiles of 17 major Raman lines of $Mn^{III}Mb{\cdot}N_3^-$ (250 mM azide ion concentration), including the modes at 170, 282, 650, and 2039 cm^{-1}, which are absent without azide ion. All porphyrin ring modes except the one at 795 cm^{-1} exhibit clear 0–0 peaks at ~470 nm (band V maximum), indicative of significant vibronic couplings with the band V excited state. The feature of increasing scattered intensity toward higher energies after the initial 0–0 peaks is similar to that reported by Shelnutt et al. (1976) on manganese(III) etioporphyrin I. On the other hand, the excitation profiles of bound azide modes at 650 and 2039 cm^{-1} show "expected maxima" between band V and band VI, i.e., at ~430 nm.

The totally symmetric azide stretch at 1344 cm^{-1} does not exhibit a peak at band V maximum (not shown). Because of the overlapping porphyrin ring mode at 1345 cm^{-1} (Figure 7), we were unable to determine if the slight resonance enhancement upon excitation at 457.9 nm is due to ring mode or azide mode. We believe that the observed intensity at 1344 cm^{-1} does not have an appreciable contribution from bound

Table I: Comparison of Geometrical Data between Manganese and Iron Tetraphenylporphyrin Complexes[a]

	L_1	$M-L_1$	C_t-L_1	L_2	$M-L_2$	C_t-L_2	$M-C_t$	$M-N_p$	ref
$Mn^{III}TPP(Cl^-)(Py)$	pyridine	2.444	2.32	Cl^-	2.467	2.59	0.12	2.009	*b*
$Mn^{III}TPP(Cl^-)$				Cl^-	2.373	2.638	0.265	2.008	*c*
$Mn^{III}TPP(N_3^-)(CH_3OH)$	CH_3OH	2.329	2.244	N_3^-	2.176	2.261	0.085	2.031	*d*
$Mn^{III}TPP(N_3^-)$				N_3^-	2.045	2.279	0.234	2.005	*e*
$Mn^{III}TPP(NMeIm)_2$	NMeIm	2.308		NMeIm	2.308			2.014	*f*
$Fe^{III}TPP(Cl^-)$				Cl^-	2.192	2.57	0.38	2.049	*g*
$Fe^{III}TPP(SCN^-)$				SCN^-	1.957	2.442	0.485	2.065	*c*
$Fe^{III}TPP(N_3^-)(Py)$	pyridine	2.085	2.055	N_3^-	1.926	1.956	0.03	1.990	*c*
$Fe^{III}TPP(N_3^-)$				N_3^-	1.909	2.25	0.34	2.055	*c*
$Fe^{III}TPP(Im)_2^+(Cl^-)$	Im	1.957	1.948	Im	1.991	2.000	0.009	1.989	*h*
$Mn^{II}TPP(NMeIm)$				NMeIm	2.192	2.707	0.515	2.128	*i*
$Fe^{II}TPP(2\text{-}MeIm)$				2-MeIm	2.161	2.581	0.42	2.086	*c, j*

[a] Abbreviations used: TPP, tetraphenylporphyrin; Py, pyridine; NMeIm, *N*-methylimidazole; Im, imidazole; L_1 and L_2, axial ligands; M, metals; C_t, the center of the four pyrrole nitrogens; N_p, pyrrole nitrogens. All distances are given in angstroms. [b] Kirner & Scheidt (1975). [c] Hoard (1975). [d] Day et al. (1974). [e] Day et al. (1975). [f] Scheidt (1978). [g] Hoard et al. (1967). [h] Countryman et al. (1969); Collins et al. (1972). [i] Gonzalez et al. (1975). [j] Hoard & Scheidt (1973).

azide (via resonance enhancement).

With excitation wavelengths at 413.1 and 406.7 nm, we noted the appearance of two new additional Raman lines at 1010 and 2006 cm^{-1}, which shifted to 983 and 1954 cm^{-1}, respectively, upon $^{15}N_3$ isotope substitution. The time-dependent increase of their intensities was still noticeable even after ~1 h of near-UV laser irradiation. Concomitant changes are the intensity increases of some porphyrin ring modes (relative to the internal standard 983-cm^{-1} sulfate line). Therefore, the data points for 650- and 2039-cm^{-1} modes were obtained within the initial 5 min of laser irradiation to minimize the formation of the photoinduced complex. Judged from the intensity ratio of the 1010-cm^{-1} mode to the internal standard at 983 cm^{-1} within ~5 min of irradiation (406.7 nm, 10 mW, at sample point), the photoinduced complexes are less than 10% of the total MnMb–azide complexes. For wavelengths other than 406.7 and 413.1 nm, we could not observe any time dependence of Raman lines; even the sample was irradiated for 2–3 h. The nature of the photoinduced new MnMb–azide complex is under active investigation in our laboratory.

Discussion

(*a*) *Lower Frequency Modes.* The iron–proximal histidine bond [Fe–N_ϵ(His)] is an important chemical link in the function of heme proteins. Recently, several groups of investigators have made attempts to identify a low-frequency RR line, which may be reasonably ascribed as Fe–N_ϵ(His) stretch. Desbois et al. (1979) assigned the 411-cm^{-1} line to the Fe(III)–N_ϵ(His) stretch in the Soret-excited RR spectra of $Fe^{III}Mb{\cdot}H_2O$ on the basis that this line was not observed in the infrared spectra of metalloporphyrins or in the RR spectra of iron(III) mesoporphyrin complexes. This line shifted to 408 cm^{-1} in $Fe^{II}Mb$, which was assigned to the Fe(II)–N_ϵ(His) stretch by the same authors. To the contrary, Kitagawa et al. (1979) and Nagai et al. (1980) assigned the 220-cm^{-1} line of $Fe^{II}Mb$ and $Fe^{II}Hb$ to the Fe(II)–N_ϵ(His) stretch on the basis of a 2-cm^{-1} shift upon substitution of ^{56}Fe by ^{54}Fe. Kincaid et al. (1979a,b) favored the latter assignment after correcting their earlier one at ~370 cm. Recent work by Tsubaki et al. (1980) on the effect of heme peripheral group modifications was consistent with the assignment of Kitagawa et al. (1979). The 220-cm^{-1} line in $Fe^{II}Mb$ may correspond to the 249- or 272-cm^{-1} line in $Fe^{III}Mb{\cdot}H_2O$.

In the present study, we found a 1:1 correspondence of Raman lines between MnMb and FeMb in both oxidized and reduced states. Only several lines showed substantial shifts upon metal substitution: i.e., 252, 267, 314, and 414 cm^{-1} for oxidized states and 215 and 249 cm^{-1} for reduced states. It is reasonable to consider that these metal-sensitive modes may have larger contributions from metal–N_ϵ(His) and/or metal–N (pyrrole) stretch.

X-ray crystallographic data on several manganese(III) porphyrin complexes indicate relatively strong Mn(III)–N (pyrrole) bonds and weak Mn(III)–axial ligand interaction (Table I). All the manganese(III) porphyrin complexes show longer Mn(III)–axial ligand distance than the corresponding complexes of iron(III) porphyrin. This decrease in the force constant of the Mn–axial ligand bond is also preserved in the reduced state. In the light of this evidence and consistent with the current assignment of 220 cm^{-1} to Fe(II)–N_ϵ(His) stretch, we favor the assignment of the Mn–N_ϵ(His) stretch to the 215-cm^{-1} line for the reduced state and the 267-cm^{-1} line for the oxidized state. The downward frequency shift caused by a decrease in the force constant of metal–axial ligand [N_ϵ(His)] should surpass the upward shift caused by the mass decrease from iron to manganese. The 249-cm^{-1} line in the reduced state and the 252-, 314-, and 414-cm^{-1} lines in the oxidized state are ruled out because they show shifts toward the opposite direction.

It should be emphasized that our assignment of the Mn–N_ϵ(His) stretch as well as the assignment of 220 cm^{-1} to the Fe(II)–N_ϵ(His) stretch by Kitagawa et al. (1979) and Kincaid et al. (1979a,b) cannot be considered as "established". Uncertainities still remain, particularly the question of why the Mn(II)–N_ϵ(His) [or Fe(II)–N(His)] stretch is enhanced so strongly upon Soret ($\pi \rightarrow \pi^*$ in-plane transition) excitation. The mechanism by which the out-of-plane vibration is enhanced via an in-plane electronic transition is currently unknown.

There are two lines at 170 and 282 cm^{-1} which appear upon adding azide to $Mn^{III}Mb$. These lines, insensitive to $^{15}N_3$ isotope substitution and having no analogue to other heme protein spectra, may be tentatively assigned to the out-of-plane porphyrin ring modes, with the latter involving significant Mn(III)–N_ϵ (pyrrole) stretch. Such a stretching mode (A_1 under C_{4v}, but A_{2u} under D_{4h}) is expected to be polarized if the metal is out of plane.

(*b*) *Azide* (π) $\rightarrow$ *Porphyrin* (π^*) *Charge-Transfer Transitions.* According to the theories of resonance Raman scattering (Albrecht, 1961; Mingardi & Siebrand, 1975; Peticolas et al., 1970; Shelnutt et al., 1977), a vibrational mode may derive its resonance intensity via Franck–Condon overlaps and/or Herzberg–Teller vibronic couplings. The former mechanism is in resonance with one excited electronic state. More specifically, Albrecht's *A* and *B* terms containing overlap

factors $\langle i|v\rangle\langle v|j\rangle$ and vibronic coupling matrix elements $\langle e^\circ|(\partial H/\partial Q_a)_0|s^\circ\rangle$, respectively, may be given:

$$A_{\rho\sigma} = \sum_{e\neq g}{}' \sum_{v} \frac{M^{\sigma}_{ge} M^{\rho}_{eg} \langle i|v\rangle\langle v|j\rangle}{E_{ev} - E_{gi} - E_0 + i\Gamma_{ev}} \quad (1)$$

$$B_{\rho\sigma} = \sum_{e\neq g}{}' \sum_{v} \sum_{s\neq e} \sum_{a} \frac{\langle e^\circ|(\partial H/\partial Q_a)_0|s^\circ\rangle}{(E^\circ_e - E^\circ_s)(E_{ev} - E_{gi} - E_0 + i\Gamma_{ev})} \times [M^{\sigma}_{ge} M^{\rho}_{sg} \langle i|v\rangle\langle v|Q_a|j\rangle + M^{\rho}_{ge} M^{\sigma}_{sg} \langle i|Q_a|v\rangle\langle v|j\rangle] \quad (2)$$

where $|i\rangle$ and $|j\rangle$ are initial and final vibrational wave functions of the ground electronic state, g, and $|v\rangle$ is a vibrational wave function of the excited electronic state, e; M^{σ}_{ge} is the σ component of electronic transition moment for $g \rightarrow e$; H is the Hamiltonian for the total electronic energy of the molecule; Q_a is the ath normal coordinate of the ground electronic state; E_{gi} and E_{ev} are the energies of the states gi and ev, respectively; E_0 is the energy of incident light; and $|e^\circ\rangle$ and $|s^\circ\rangle$ are the electronic wavefunctions evaluated at the equilibrium nuclear position ($Q_a = 0$) of the ground electronic state.

When the same vibrational frequency for ground and excited states (usually a good approximation) is assumed, the Raman Franck–Condon overlap integrals $\langle i|v\rangle\langle v|j\rangle$ are nonzero if there is a shift in the equilibrium position upon excitation. When a Jahn–Teller effect in the excited state is neglected, shifts of equilibrium position only take place along totally symmetric coordinates. In other words, non totally symmetric modes cannot derive intensities from the A term.

The azide bending mode at 650 cm^{-1} and antisymmetric stretch at 2039 cm^{-1} are both depolarized and thus non totally symmetric vibrations. They are Jahn–Teller inactive in a linear molecule although the excited state of azide ion (with one electron removed) is doubly degenerate. Thus their resonance intensities must be derived from the B term, which requires vibronic couplings between excited electronic states. The excitation profiles of the 650- and 2039-cm^{-1} lines indicate the existence of a new change-transfer transition between bands V and VI in the $Mn^{III}Mb{\cdot}N_3^-$ complex. It is possible that this charge-transfer state is vibronically coupled to nearby excited states (bands V, Va, and VI), resulting in the enhancement of non totally symmetric internal azide modes and two out-of-plane porphyrin ring modes at 170 and 282 cm^{-1}. Unless the nonadiabatic effect (Shelnutt et al., 1977) is unusually large, the absence of a peak at the band V maximum in the excitation profiles of the 650- and 2039-cm^{-1} lines suggests that vibronic couplings with band V may be small. The nature of this new charge-transfer transition is likely to be of azide (π) → porphyrin (π^*) type rather than azide (π) → Mn (d_{a^2}) or azide (n) → Mn (d_{a^2}) because a transition populating the orbital (d_{z^2}) is expected to enhance the Mn–N_3 stretch, which has not been observed.

Wright et al. (1979) reported the enhancement of axial pyridine internal vibrations upon excitation into the Fe (d_π) → Py (π^*) charge-transfer band in the bis(pyridine)iron(II) mesoporphyrin IX dimethyl ester complex. In resonance with this charge-transfer state, totally symmetric (but not non totally symmetric) internal pyridine vibrations as well as the Fe(II)–pyridine stretch are greatly enhanced, consistent with the one-excited-state Franck–Condon (Albrecht's A term) scattering.

The ligation properties of manganese(III) and iron(III) heme are quite different. The cyanide ion, which binds iron(III) heme and is generally considered as a stronger ligand than azide, does not bind to manganese(III) myoglobin. The significant overlaps between the π orbitals of azide and porphyrin ring, which facilitate the charge transfer, may play an important role in the interactions. Hoffman & Gibson (1976) on the basis of their kinetic studies proposed a configuration in which the manganese ion was pulled through the central hole toward the azide with an elongated bond to the imidazole nitrogen. Examination of the RR spectra of the model complex, manganese(III) protoporphyrin IX dimethyl ester–azide, in the presence and absence of added 2-methylimidazole should provide valuable data in testing this hypothesis.

References

Alben, J. O., & Fager, L. Y. (1972) *Biochemistry 11*, 842–847.

Albrecht, A. C. (1961) *J. Chem. Phys. 34*, 1476–1484.

Asher, S. A., & Sauer, K. (1976) *J. Chem. Phys. 64*, 4115–4125.

Asher, S. A., & Schuster, T. M. (1979) *Biochemistry 18*, 5377–5387.

Asher, S. A., Vickery, L. E., Schuster, T. M., & Sauer, K. (1977) *Biochemistry 16*, 5849–5856.

Boucher, L. J. (1972) *Coord. Chem. Rev. 7*, 289–329.

Collins, D. M., Countryman, R., & Hoard, J. L. (1972) *J. Am. Chem. Soc. 94*, 2066–2072.

Countryman, R., Collins, D. M., & Hoard, J. L. (1969) *J. Am. Chem. Soc. 91*, 5166–5167.

Day, V. W., Stults, B. R., Tasset, E. L., Day, R. O., & Marianelli, R. S. (1974) *J. Am. Chem. Soc. 96*, 2650–2652.

Day, V. W., Stults, B. R., Tasset, E. L., Marianelli, R. S., & Boucher, L. J. (1975) *Inorg. Nucl. Chem. Lett. 11*, 505–509.

Deatherage, J. F., Obendorf, S. K., & Moffat, K. (1979) *J. Mol. Biol. 134*, 419–429.

Desbois, A., Lutz, M., & Banerjee, R. (1979) *Biochemistry 18*, 1510–1518.

Gaughan, R. R., Shriver, D. F., & Boucher, L. J. (1975) *Proc. Natl. Acad. Sci. U.S.A. 72*, 433–436.

Gonzalez, B., Kouba, J., Yee, S., Reed, C. A., Kirner, J. F., & Scheidt, W. R. (1975) *J. Am. Chem. Soc. 97*, 146–151.

Hoard, J. L. (1975) in *Porphyrins and Metalloporphyrins* (Smith, K. M., Ed.) pp 317–380, Elsevier, Amsterdam.

Hoard, J. L., & Scheidt, R. (1973) *Proc. Natl. Acad. Sci. U.S.A. 70*, 3919–3922.

Hoard, J. L., Cohen, G. H., & Glick, M. D. (1967) *J. Am. Chem. Soc. 89*, 1992–1996.

Hoffman, B. M., & Gibson, Q. H. (1976) *Biochemistry 15*, 3405–3410.

Jones, K. (1973) in *Comprehensive Inorganic Chemistry* (Trotman-Dickenson, A. F., Ed.) Vol. 2, Chapter 19, pp 276–293, Pergamon Press, New York.

Kincaid, J., Stein, P., & Spiro, T. G. (1979a) *Proc. Natl. Acad. Sci. U.S.A. 76*, 549–552.

Kincaid, J., Stein, P., & Spiro, T. G. (1979b) *Proc. Natl. Acad. Sci. U.S.A. 76*, 4156.

Kirner, J. R., & Scheidt, R. (1975) *Inorg. Chem. 14*, 2081–2090.

Kitagawa, T., Nagai, K., & Tsubaki, M. (1979) *FEBS Lett. 104*, 376–378.

McCoy, S., & Caughey, W. S. (1970) *Biochemistry 9*, 2387–2393.

Mingardi, M., & Siebrand, W. S. (1975) *J. Chem. Phys. 62*, 1074–1085.

Moffat, K., & Hoffman, B. M. (1976) *J. Mol. Biol. 104*, 669–685.

Nagai, K., Kitagawa, T., & Morimoto, H. (1980) *J. Mol. Biol. 136*, 271–289.

Ogoshi, H., Watanabe, E., Yoshida, Z., Kincaid, J., & Nakamoto, K. (1973) *J. Am. Chem. Soc. 95*, 2845–2849.

Perutz, M. F., & Mathews, F. S. (1966) *J. Mol. Biol. 21*, 199–202.
Peticolas, W. L., Nafie, L., Stein, P., & Fanconi, B. (1970) *J. Chem. Phys. 52*, 1576–1584.
Scheidt, W. R. (1978) *Porphyrins 3*, 463–511.
Shelnutt, J. A., O'Shea, D. C., Yu, N.-T., Cheung, L. D., & Felton, R. H. (1976) *J. Chem. Phys. 64*, 1156–1165.
Shelnutt, J. A., Cheung, L. D., Chang, R. C. C., Yu, N.-T., & Felton, R. H. (1977) *J. Chem. Phys. 66*, 3387–3398.
Sono, M., & Asakura, T. (1975) *J. Biol. Chem. 250*, 5227–5232.
Spaulding, L. D., Chang, R. C. C., Yu, N.-T., & Felton, R. H. (1975) *J. Am. Chem. Soc. 97*, 2517–2525.
Spiro, T. G., & Strekas, T. C. (1974) *J. Am. Chem. Soc. 96*, 338–345.
Spiro, T. G., Stong, J. D., & Stein, P. (1979) *J. Am. Chem. Soc. 101*, 2648–2655.
Stryer, L., Kendrew, J. C., & Watson, H. C. (1964) *J. Mol. Biol. 8*, 96–104.
Teale, F. W. J. (1959) *Biochim. Biophys. Acta 35*, 543.
Tsubaki, M., Nagai, K., & Kitagawa, T. (1980) *Biochemistry 19*, 379–385.
Wright, P. G., Stein, P., Burke, J. M., & Spiro, T. G. (1979) *J. Am. Chem. Soc. 101*, 3531–3535.
Yonetani, T., & Asakura, T. (1969) *J. Biol. Chem. 244*, 4580–4588.
Yu, N.-T. (1977) *CRC Crit. Rev. Biochem. 4*, 229–280.
Yu, N.-T., & Srivastava, R. B. (1980) *J. Raman Spectrosc. 9*, 166–171.

Amino Acid Sequence of a Collagenolytic Protease from the Hepatopancreas of the Fiddler Crab, *Uca pugilator*†

Gregory A. Grant,* Kenneth O. Henderson, Arthur Z. Eisen, and Ralph A. Bradshaw

ABSTRACT: The amino acid sequence of a collagenolytic protease from the hepatopancreas of the fiddler crab, *Uca pugilator*, was determined from the structures of overlapping tryptic, chymotryptic, thermolytic, staphylococcal protease, and cyanogen bromide peptides together with automated sequencer analysis of the intact protein. Crab collagenase is a serine protease composed of 226 residues which is capable of degrading the native triple helix of collagen under physiological conditions. When aligned for optimal homology, crab collagenase displays 35% identity with bovine trypsin, 38% with bovine chymotrypsin B, and 32% with porcine elastase. The six half-cystinyl residues in crab collagenase correspond to those forming three of the five disulfide bonds in chymotrypsin. The residues forming the charge relay system of the active site of chymotrypsin (His-57, Asp-102, and Ser-195) are found in corresponding regions in crab collagenase, and the sequences around these residues are well conserved. The primary structure of crab collagenase is the first reported for a serine protease from crustacean hepatopancreas and the first reported for a serine protease possessing the unusual property of being able to degrade native helical collagen.

The proteolytic enzyme isolated from the hepatopancreas of the fiddler crab, *Uca pugilator* (Eisen & Jeffrey, 1969; Eisen et al., 1970, 1973), is capable of degrading collagen under conditions that do not denature the protein and is characterized by the cleavage of the native collagen helix at several sites in the area of the TC^{A}_{75} locus of the molecule (Eisen & Jeffrey, 1969). Unlike vertebrate collagenases, however, the crab hepatopancreas collagenase exhibits trypsin- and chymotrypsin-like activities, determined with synthetic substrates, as inherent properties of the same molecule (Eisen et al., 1973). In addition, this collagenolytic protease resembles the vertebrate serine proteases with respect to inhibition by diisopropyl fluorophosphate and soybean trypsin inhibitor, pH optimum, and approximate molecular weight (ca. 25000) (Eisen et al., 1973).

The complete amino acid sequence of this enzyme has been determined from overlapping cyanogen bromide, tryptic, chymotryptic, thermolytic, and *Staphylococcus aureus* V8 protease peptides. The sequence unequivocally demonstrates that this collagenolytic enzyme is a serine protease of the trypsin family. In this respect, it differs from vertebrate collagenases which are zinc metalloenzymes (Seltzer et al., 1977) and is unique in that no other known serine protease is capable of degrading the native triple helix of collagen. This sequence is the first reported for a serine protease from crustacean hepatopancreas.

Materials and Methods

The enzyme was obtained from live fiddler crabs as previously described (Eisen et al., 1973). L-1-(Tosylamido)-2-phenylethyl chloromethyl ketone treated trypsin, chymotrypsin, and carboxypeptidases A and B were purchased from Worthington Biochemical Corp. Thermolysin was purchased from Calbiochem and *S. aureus* V8 protease from Miles. Carboxypeptidase Y and phenyl isothiocyanate for manual sequencing were obtained from Pierce Chemical Co. *o*-Iodosobenzoate was purchased from Chemical Dynamics and β-mercaptoethanol from Eastman. Iodoacetic acid, trifluoroacetic acid, and dansyl chloride were purchased from Sigma Chemical Co., and cyanogen bromide and diisopropyl fluorophosphate were from Aldrich Chemical Co. Iodo-[^{14}C]acetic acid was obtained from New England Nuclear,

† From the Division of Dermatology, Department of Medicine (G. A.G., K.O.H., and A.Z.E.), and the Department of Biological Chemistry (G.A.G. and R.A.B.), Washington University School of Medicine, St. Louis, Missouri 63110. *Received April 3, 1980.* This investigation was supported by U.S. Public Health Service Grants AM 13362, AM 12129, and AM 07284.

0006-2960/80/0419-4653$01.00/0